



Investigation of the hepatotoxicity of flutamide: Pro-survival/apoptotic and necrotic switch in primary rat hepatocytes characterized by metabolic and transcriptomic profiles in microfluidic liver biochips

Audrey Legendre, Sébastien Jacques, Florent Dumont, Jérôme Cotton,
Patrick Paullier, Marie José Fleury, Eric Leclerc

► To cite this version:

Audrey Legendre, Sébastien Jacques, Florent Dumont, Jérôme Cotton, Patrick Paullier, et al.. Investigation of the hepatotoxicity of flutamide: Pro-survival/apoptotic and necrotic switch in primary rat hepatocytes characterized by metabolic and transcriptomic profiles in microfluidic liver biochips. *Toxicology in Vitro*, 2014, 28 (5), pp.1075-1087. 10.1016/j.tiv.2014.04.008 . hal-03820688

HAL Id: hal-03820688

<https://hal.science/hal-03820688>

Submitted on 1 Aug 2023

HAL is a multi-disciplinary open access archive for the deposit and dissemination of scientific research documents, whether they are published or not. The documents may come from teaching and research institutions in France or abroad, or from public or private research centers.

L'archive ouverte pluridisciplinaire **HAL**, est destinée au dépôt et à la diffusion de documents scientifiques de niveau recherche, publiés ou non, émanant des établissements d'enseignement et de recherche français ou étrangers, des laboratoires publics ou privés.



Distributed under a Creative Commons Attribution - NonCommercial - NoDerivatives 4.0
International License

**Investigation of the hepatotoxicity of flutamide: pro-survival/apoptotic and
necrotic switch in primary rat hepatocytes characterized by metabolic and
transcriptomic profiles in microfluidic liver biochips**

Audrey Legendre¹, Sébastien Jacques², Florent Dumont², Jérôme Cotton³, Patrick
Paullier¹, Marie José Fleury¹, and Eric Leclerc^{1*}

¹ CNRS UMR 7338, Laboratoire de Biomécanique et Bio ingénierie, Université de
Technologie de Compiègne, France

² INSERM U1016 Plate-forme génomique institut Cochin, 22 rue Méchain, 75014 Paris,
France

³ Profilomic, 31 rue d'Aguesseau, 92100, Boulogne-Billancourt, France

*Correspondence should be addressed to:

Eric Leclerc

CNRS UMR 7338, Laboratoire de Biomécanique et Bioingénierie, Université de
Technologie de Compiègne, France

Email: eric.leclerc@utc.fr

Phone: 33 (0)3 44 23 79 43

Abstract

We investigated the effects of the liver damage induced by flutamide in primary rat hepatocytes using liver microfluidic biochips. Flutamide is a non-steroidal anti-androgenic drug. Two flutamide concentrations, 10 μ M and 100 μ M, were used to expose the hepatocytes for 24h under perfusion. Thanks to the maintenance of hepatocyte differentiation phenotype and to the biotransformation performance in the microfluidic cultures, the metabolic ratio analysis of hydroxyflutamide, flutamide-gluthatione and hydroxyflutamide-gluthatione productions demonstrated saturation of the drug's biotransformation process and the maintenance of a high level of flutamide at 100 μ M when compared to 10 μ M. A microarray analysis comparing flutamide (10 or 100 μ M) with controls revealed a common response for both concentrations illustrated by modulating the expression of the mRNA of genes associated with mitochondrial perturbation, of the proliferator-activated receptors (*Ppar*) signaling, lipid and fatty acid metabolism, antioxidant defense, and cell death pathways, consistently with *in vitro* and *in vivo* reports. Additionally to literature reports, our integration of the transcriptomic profiles demonstrated a specific dose dependent response. We found at 10 μ M a typical pro-survival/apoptosis network activation (through *IGF/PDGFD* upstream route and *via* a downstream up regulation in *CREB5*, *BCL2*, *IKBKG* routes in the PI3K/signaling). We also found a down regulation of mRNA levels in sugar and amino acid metabolism pathways. At 100 μ M a typical necrosis switch was observed associated with a down regulation of the tight junctions' pathway, a cellular aggregation and a reduction of the cell viability. Altogether our data demonstrated the potential and the sensitivity of our liver microfluidic cultures to evaluate xenobiotic toxicity by improving *in vitro* analysis and reproducing both *in vitro* and *in vivo* results. Finally, we proposed two integrated synthetic networks to describe the response of rat hepatocytes to both exposure concentrations of flutamide.

Keywords: Microfluidic biochips, rat primary hepatocytes, flutamide, hepatotoxicity, transcriptomic, microarray, metabolism

1. Introduction

Pharmaceutical companies are facing an Research and Development (R&D) productivity crisis with ever increasing drug development costs and time to market. A large part of the problem lies in high failure rates of drugs during the expensive clinical trial phase (Bains, 2004). Currently ~90% of all drugs that enter clinical trials end up failing due to unpredicted toxicity (~30%), low efficacy (~40%) and Absorption Distribution Metabolism Elimination (ADME) profile (~10%). The test methods available (traditional *in vitro*, *in vivo*, *ex vivo* and *in silico*) are not accurate enough (e.g. traditional *in vitro*) and/or not practical enough (e.g. *ex vivo*) for pharmaceutical companies to improve prediction for the human condition, and thus make better decisions earlier on in the process. At the same time, chemical, cosmetics and personal care companies are facing increasingly strict regulations regarding animal trials – with a ban already in place for cosmetics in Europe. For many test endpoints there are no sufficiently accurate alternatives to animal trials and both the industry and its regulators are keen to find alternatives.

The new technology provided by microfluidic liver biochips can, for several important application areas, meet this unmet need in pharmaceutical companies as well as chemicals, cosmetics and personal care industries. By replicating key aspects of *in vivo* conditions, such as three dimensional cell structures (Powers *et al.*, 2002), circulatory flow (Baudoin *et al.*, 2011) and zonation (Tilles *et al.*, 2001; Cheng *et al.*, 2012), multi organs (Viravaydia *et al.*, 2004; Choucha *et al.*, 2013a) or multi cellular co-cultures (Novik *et al.*, 2010), leading to a closer representation when compared to traditional *in vitro* methods, the human-like environment can be mimicked. The concept of the technology consists of a micro environment for dynamic three dimensional microstructure cell cultures that become “bioartificial organs” capable of simulating human physiology. Within this context, our group has developed an integrated platform, the IDCCM box (for Integrated Dynamic Cell Culture in Microsystems), which makes parallel connection of biochips possible, thus increasing throughput and facilitating the investigations (Baudoin *et al.*, 2012; 2013).

Functionality and the potential for hepatic metabolism in such biochips have been illustrated *via* analysis of phases I and II xenobiotic metabolism-related genes and by

84 drug clearances and biotransformation (Chao *et al.*, 2009; Baudoin *et al.*, 2013;
85 Legendre *et al.*, 2013). In addition, more in-depth investigations of hepatotoxicity have
86 also been made possible thanks to the compatibility of liver biochip cultures with
87 conventional biochemical analysis processes such as metabolomics, proteomics and
88 transcriptomics (Shintu *et al.*, 2012; Prot *et al.*, 2011a, 2012). Thus, basal analysis on
89 primary rat hepatocytes and human liver cell lines has shown that cell defense
90 mechanisms including drug metabolism were over expressed in the microfluidic liver
91 biochips (Prot *et al.*, 2011b, Legendre *et al.*, 2013). When applied to acetaminophen
92 injury with cell lines, this led to reproducing a substantial sequence of the mechanism of
93 actions when compared to Petri analysis (Prot *et al.*, 2012).

94 In order to investigate the effect of drug treatment, we focused our study on the
95 non-steroidal anti-androgenic drug, flutamide. Flutamide is one of several beneficial
96 drugs used in the treatment of prostate cancer and in combination with oral
97 contraceptives for the treatment of hirsutism and benign prostatic hyperplasia (Wang *et al.* 2002). In prostate cancer, tumor cells need testosterone to proliferate. Flutamide and
98 its active metabolite, 2-hydroxyflutamide, compete with testosterone to bind to androgen
99 receptors leading to impairment of testosterone signaling and modulation of the
100 testosterone-dependent pathways. However, flutamide presents secondary toxicity in
101 the liver. The mechanisms for liver damage associated with flutamide use are currently
102 unknown, with many hypotheses for the mechanisms liable to play a part in the liver
103 damage (e.g. P450-mediated bioactivation, mitochondrial dysfunction, generation of
104 reactive oxygen species (ROS), inhibition of the bile salt transporter; Coe *et al.*, 2006;
105 2007, Iwanaga *et al.*, 2007). In addition, the toxicity of flutamide is also due to the
106 production of hydroxyflutamide *via* the cytochrome P450-1A (CYP1A) biotransformation
107 (Schulz *et al.* 1988, Shet *et al.*, 1997). More particularly, flutamide was reported to have
108 human hepatotoxic properties in post-marketing studies (Aizawa *et al.*, 2003, Coe *et al.*,
109 2006). The precise mechanism behind hepatic dysfunction in humans has not yet been
110 clarified because it is probably the result of metabolic idiosyncrasy (Aizawa *et al.*, 2003,
111 Coe *et al.*, 2006; 2007).

112
113 The plasmatic concentrations of flutamide and hydroxyflutamide after therapeutic
114 doses ranging from 250mg to 750mg of flutamide have shown maximal values varying

between 0.4 and 3 μ M for flutamide and 3-10 μ M for hydroxyflutamide (Schulz *et al.*, 1988; Radwanski *et al.*, 1989; Anjum *et al.*, 1999). The *in vitro* IC₅₀ of flutamide (including some data extracted in microchip cultures, Zhang *et al.*, 2011), is reported to range between 30 to 90 μ M for 24h of exposure according to the culture methods and assays used (total protein synthesis in Kostrubsky *et al.*, 2007; live dead assays in Zhang *et al.*, 2011). In addition, primary rat hepatocyte exposure (0.36 to 1 μ M) led to an increase in CYP1A2 mRNA levels, aspartate aminotransferase (AST) and alanine aminotransferase (ALT) activities, and reduced glutathione (GSH) contents (Wang *et al.*, 2002).

In order to investigate low and high dose effects of flutamide and to enhance the knowledge on the potential mechanisms of hepatotoxicity, we have exposed rat hepatocytes in microfluidic conditions for 24h to 10 and 100 μ M concentrations of flutamide. The selection of those doses was based on the *in vivo* and *in vitro* data described above. Hepatocellular functions were evaluated in terms of glucose consumption, urea and albumin secretions. The metabolism performance of the hepatocytes was also confirmed by metabolite detection and CYP1A activity. The transcriptomic profile was then analyzed in order to identify the mechanism of action of flutamide in microfluidic biochips. Finally the data was compared with literature reports.

2. Material and methods

2.1 IDCCM bioreactor

The entire culture set-up was called the IDCCM for “Integrated Dynamic Cell Culture in Microsystems”. The concept and details of the IDCCM box and biochips are presented in detail in our previous work (Baudoin *et al.*, 2011; 2012). Briefly, the polydimethylsiloxane (PDMS) biochips were connected to the bottom of the IDCCM box by a simple series of “plugging” ports (Fig 1A). This format made for an easy “plug and display” of the biochips in external set-ups such as microscopes. The IDCCM is a manufactured polycarbonate box using the conventional format of the 24-well plate. Each microfluidic biochip is connected between two wells. The 24 wells were used as an

inlet and outlet reservoir leading to the parallelized culture of 12 biochips (Fig 1B). A specific cover was designed so that the polycarbonate box could be closed hermetically for continuous flow perfusion. The cover included ports for fluid perfusion and sampling. The hermetic closure of the IDCCM box and the pressure in the IDCCM box prevented any leakage or reservoir drain.

2.2 Primary rat hepatocyte cultures in the IDCCM

The hepatocytes extraction is given in detail in the supplementary file 1 and in our previous work (Legendre et al. 2013). The experiments were performed over a period of 48h which included three different phases: hepatocyte extraction (day-0, post extraction), the adhesion phase (day-1, 24h of adhesion), which was performed at 37°C, and a 24h perfusion phase at 32°C (Fig 1C). The sterilization of the biochips, the IDCCM box and the perfusion circuit was achieved by autoclaving the whole set-up. The biochips were then connected to the box under sterile conditions.

Freshly isolated hepatocytes were cultured for the first 24 hours in a seeding medium composed of William's E Glutamax medium (Fisher Scientific, Illkirch, France) supplemented with bovine insulin (5µg/ml, Sigma-Aldrich, Saint-Quentin Fallavier, France) and fetal bovine serum (10%v/v). To enhance cell adhesion, the inner surface of the biochips was coated with rat tail type 1 collagen (0.3mg/ml, BD Biosciences) prepared in phosphate-buffered saline (PBS) for 1 hour at 37°C in a humidified atmosphere supplied with 5% CO₂. After washing with the seeding medium, the cells were inoculated inside the biochips at 0.5×10⁶ cells per biochip (*i.e.* 0.25×10⁶ per cm²). After the 24h adhesion period, cells were cultured in DMEM-F12 medium (Fisher Scientific) supplemented with 15mM Hepes, 1.2g/L sodium bicarbonate (Sigma-Aldrich), 6.25µg/ml insulin-transferrin-selenium solution (Becton Dickinson, Biosciences, Le Pont de Claix, France), 100 units/ml of penicillin and 100mg/ml of streptomycin (Fisher Scientific).

The IDCCM was prepared for the perfusion phase. Medium reservoirs at the inlet and outlet were filled with a volume of 2mL of culture medium to ensure the correct

medium supply during dynamic culture resulting in a total volume of 4mL for each biochip. Then, the polytetrafluoroethylene (PTFE) tubes were connected to the fluidic cover of the IDCCM box and to the peristaltic pump. PTFE tubes were used for maximum prevention of the loss of chemical compounds through diffusion or adsorption to the tubing in the fluidic circuit. The entire system (pump and IDCCM box with the biochips) was placed in the incubator (32°C, 5% CO₂) and the perfusion was started (25µl/min flow rate). Culture medium was sampled and stocked at -20°C for posterior assays. Cytochrome assays and cell counting were performed on the biochips (see below). The cells were photographed using a Leica DMI 6000B microscope together with the Leica camera and LAS life software (Leica Microsystems).

2.3 Cellular assays

Details of the protocols of the cellular assays are presented in supplementary file 1 and in our previous works (Baudoin et al., 2011; 2012, Choucha Snouber et al., 2013). Briefly, cell counting was performed on a Malassez cell following cell detachment with trypsin-EDTA (Fisher Scientific). Cell viability was quantitatively analyzed using trypan blue staining. Functional metabolism was analysed using CYP1A2 activity, glucose consumption, urea and albumin productions. CYP1A2 activity was determined using 5-ethoxyresorufin (10µM) as the substrate. Glucose consumption and urea production were analyzed using a biochemical analyzer, the Konelab 20 (Thermo Fisher Electron Corporation, Courtaboeuf, France). Albumin was measured using an ELISA sandwich test in a 96-well plate according to the rat albumin ELISA Quantitation Set protocol (Bethyl Laboratories, Euromedex, Souffelweyersheim, France). Then, cell viability and necrosis was assessed by double staining using calcein AM (2µM) and propidium iodide (PI) (10µg/mL). Finally reactive oxygen species (ROS) were detected by DCFDA staining. Those stainings were performed in the biochip at the end of the perfusion in control and flutamide treated conditions.

2.4 Transcriptomic analysis

Total RNA was extracted using the Nucleospin® RNA XS isolation kit (Macherey-Nagel EURL, Hoerd, France). The quantity and quality of the RNA were evaluated using a Nanodrop ND-1000 spectrophotometer (Nyxor Biotech, Paris, France) and the Agilent 2100 Bioanalyzer (using the Agilent RNA 6000 Nano and Pico kits), respectively. All RNA samples had an RNA Integrity Number of more than 8 (between 9.3 and 10). cDNA was synthesized from 500ng of total RNA with oligodT Primer, using SuperScript II (Life Technologies), according to the manufacturer's protocol.

After validating the quality of the RNA with Bioanalyzer 2100 (using the Agilent RNA6000 nano chip kit), 5 ng of total RNA was reverse transcribed in accordance with the Ovation PicoSL WTA System (Nugen). Briefly, the resulting double strand cDNA was used for amplification based on SPIA technology. After purification according to the Nugen protocol, 2 µg of single strand DNA were used to generate target DNA using the Ovation Exon Module kit (Nugen). 4 µg of target DNA were fragmented and biotin labeled using the Encore Biotin Module kit (Nugen). After controlling fragmentation using the Bioanalyzer 2100, cDNA was then hybridized to GeneChip® Rat Gene 1.0 ST (Affymetrix) at 45°C for 17 hours.

After overnight hybridization, the chips were washed on the fluidic station FS450 following specific protocols (Affymetrix) and scanned using the GCS3000 7G. The scanned images were then analyzed with Expression Console software (Affymetrix) to obtain raw data (.cel files) and metrics for Quality Control. The observations of some of these metrics and the study of the distribution of raw data did not reveal any out-of-range experiments.

2.5 Bioinformatics

2.5.1 Quality assessments, normalization and statistics

The raw data were normalized using the Robust Multichip Algorithm (RMA) in the Bioconductor R. All quality controls and statistics were then carried out using Partek GS®. First we established hierarchical clustering (Pearson's dissimilarity and average linkage) and Principal Component Analysis to control the data. To find differentially expressed genes, we used a classic variance analysis for each gene and made paired

Tukey's *post hoc* tests between groups. We then used p-values and fold changes to filter and select differentially expressed genes.

2.5.2 Functional analysis

Interactions, pathways and functional enrichment analyses were carried out using the IPA (Ingenuity® Systems, USA www.ingenuity.com) and KEGG (Kyoto Encyclopedia of Genes and Genomes) databases.

2.6 Mass Spectrometry analysis

To detect and confirm the metabolism of flutamide into hydroxyflutamide and the glutathione conjugations by the hepatocytes in the microfluidic biochips, we performed an additional mass spectrometry analysis. Detailed protocol is given in supplementary file 1 and in our previous works (Baudoin et al. 2014). To achieve our internal quality criteria the quantification of positively identified analytes was made using an external calibration curve in blank matrix. Nine standards concentrations corresponding to 0.1 ng/mL, 1 ng/mL, 5 ng/mL, 10 ng/mL, 50 ng/mL, 100 ng/mL, 500 ng/mL, 1000 ng/mL and 5000 ng/mL with three replicated injections were carried out for build of the calibration curve of flutamide and hydroxyflutamide. The quantification was considered valid only within the measured linear range. Thanks to these standard curves, flutamide and hydroxyflutamide concentrations were estimated. The HF metabolic ratio was defined by the ratio between the hydroxyflutamide and the flutamide concentrations. Concerning the flutamide metabolites identified by the fragmentation experiments, a metabolic ratio was calculated using the area under curves (AUC) ratio.

2.7 Statistic analysis

Three independent experiments (i.e 3 euthanized rats) were assessed. Each experiment was repeated at least three times in triplicate biochips. Data were plotted as mean \pm the standard error of the mean (SEM). Statistical analyses were performed by unpaired t test using GraphPad statistical analysis (Prism 5, version 5.02). The

statistically significant differences are reported on the histograms and tables (**
P<0.001, ** P<0.01, * P<0.05).

3. Results

3.1 Morphology and cell viability of rat hepatocytes in IDCCM biochips after flutamide treatment

The hepatocyte morphologies at the end of the experiments (after adhesion and after 24h of perfusion) in control, with 10µM and 100µM of flutamide are presented in Fig. 2A to 2C. The hepatocytes adhered and covered the microfluidic channels. After 24h of perfusion, the control and the 10µM treated biochips presented similar morphologies. The hepatocytes were refringent between their cell junctions, with a typical cuboid shape. The hepatocyte-like morphology was conserved over time and the hepatocytes were still located in the biochips, forming a dense cell layer. At 100µM, the hepatocytes were less dense and were not confluent. Finally, no difference was observed between the counted cell in control and 10 µM-flutamide biochips. The number of hepatocytes was greatly decreased after 100µM flutamide treatment, resulting in a significant reduction of 35% of the total collected cells (Fig. 3A).

3.2 Basal metabolism of rat hepatocytes in IDCCM biochips after flutamide treatment

Mitochondrial respiration was assessed using the alamar blue kit. It revealed intense mitochondrial activity with flutamide treatments which was statistically different from the controls. Both 10µM and 100µM flutamide exposures led to an increase of up to 60% of the mitochondrial metabolism (Fig. 3B). The glucose consumption and urea production increased when the flutamide concentration increased and significant differences were observed in comparison with control cultures (Figs. 3C and 3D). However, we did not detect any effect on albumin (Figs 3D and 3E).

3.3 Drug metabolism of rat hepatocytes in IDCCM biochips after flutamide treatment

CYP1A is the major cytochrome P450 involved in the flutamide metabolism. The hepatocyte metabolism performances were confirmed by EROD biotransformation (EROD being a CYP1A substrate). The levels of resorufin production increased when the flutamide concentration increased (Fig. 3F). In addition, the mass spectrometry analysis confirmed, in both the 10 μ M and 100 μ M treatments, the production of the hydroxyflutamide metabolite. We estimated a production of hydroxyflutamide of 14 \pm 10 and 9 \pm 1 ng/h/10⁶cells (n=6) after 24h of perfusion during the exposures of 10 μ M and 100 μ M of flutamide respectively. The hydroxyflutamide metabolic ratio was found equal to 18.7% and 2.7% for the 10 μ M and 100 μ M flutamide exposures respectively.

Further research into the data was performed (overall value of full scan analysis) on the exact masses of flutamide and hydroxyflutamide complexed with glutathione in negative mode at 580.13306 and 596.12797 respectively. The flutamide-glutathione and the hydroxyflutamide-glutathione conjugates were identified (Supplement Fig. 1). The area under curve (AUC) analysis showed similar metabolism of glutathione conjugates for both flutamide treatments. This led to hypothesis a higher metabolic ratios for glutathione adducts when 10 μ M of flutamide was loaded when compared to 100 μ M conditions.

Finally, additional stainings were performed to evaluate the cell viability and the presence of the reactive oxygen species. In control and 10 μ M-treated biochips, the level of fluorescence of propidium was weak and corresponded to background noise. At 100 μ M, the cell population was stained positively illustrating important proportion of necrotic cells (Fig 4A to 4B). The DCFDA stainings showed that the level of ROS were high in experiments performed at 100 μ M whereas few ROS positive cells were detected at 10 μ M. Any DCFDA positive cells were observed in control (Figs 4E – 4 F).

3.4 Transcriptomic analysis

The transcriptomic analysis performed by microarray revealed a difference at the mRNA level between the treated and control conditions. The selected working gene lists from the transcriptomic analysis resulted from two subsequent mathematical selections. A first selection was applied *via* a criterion based on a *p-value* of less than 0.05. The comparisons between 10μM-treated biochips and controls (10vsctrl), and between the 100μM-treated biochips and the controls (100vsctrl) resulted to perturb respectively 2,597 and 1,553 genes. Then, to refine the lists, a second selection was performed by using a fold change criterion. Filtering with a fold change value of ± 1.5 , we reduced the two lists to 899 and 471 genes respectively for the 10vsctrl and 100vsctrl conditions (Supplement Tables 1 and 2). 252 genes were common to both flutamide exposures. In order to identify the significantly affected genes pathways and networks, these lists were analyzed with Ingenuity Pathway Analysis (IPA) and Kegg databases.

The IPA applied to the 10vsctrl comparison highlighted the “LPS/IL-1 mediated inhibition of RXR function”, “Acute Phase Response Signaling”, “Xenobiotic metabolism signaling”, “Positive Acute Phase Response Proteins”, and “Fatty acid metabolism” as the main modulated pathways (Table 1). In addition, IPA identified the following upstream regulators: *LEP*, *PPARA*, *ACOX1*, *HNF4A* and *HNF1A* (IPA *p-values* are 1.09×10^{-8} , 1.75×10^{-8} , 2.18×10^{-8} , 8.03×10^{-7} , 1.03×10^{-6} respectively). When applied to the 100vsctrl comparison, IPA extracted a modulation in the pathways “LPS/IL-1 mediated inhibition of RXR function”, “Acute Phase Response Signaling”, “Complement system”, “LXR/RXR activation”, “Fatty acid beta oxidation I and Fatty acid metabolism”, and “Cytochrome P450 panel related to Fatty acid” (Table 1). The related upstream regulators were *PPARA*, *POR*, *LEP*, *HNF4A* and *ACOX1* (IPA *p-values* are 3.8×10^{-28} , 1.25×10^{-12} , 6.49×10^{-11} , 5.72×10^{-9} , 9.96×10^{-9} respectively).

The treatments using Kegg databases complemented the results found with IPA. Running the database for the “Human+Disease/Drug” conditions, we extracted 73 and 30 pathways with at least 5 genes modulated in the pathway for the 10vsctrl and 100vsctrl gene lists respectively (Supplement Tables 3 and 4). In order to elicit a mechanistic interpretation for each flutamide treatment (10μM and 100μM), we have represented these pathways in a network of pathways by using common genes as

bridges (Figs 5 and 6). The networks created a topology of pathways in the biochips cultures. The bioinformatics treatment and the Kegg analysis extracted for both flutamide treatments the activation of cell survival pathways (*via* JAK-STAT, PI3K/AKT, MAPK, signalings, Figs 5A and 5B, table 2) and a down regulation of mRNA levels in the Ppar signaling and fatty acid metabolism (Fig 5C and 5B, table 3), drug and glutathione metabolisms (table 3).

Specific modulations were found for both 10 and 100 μ M conditions. In the 10vsctrl comparisons, cell survival was more considerably affected when compared to the situation extracted at 100vsctrl (Figs 4A and 4B, table 3). We found at 10 μ M a cell survival response through an *IGF/PDGFD* upstream route and *via* a downstream up regulation in *CREB5*, *BCL2*, *IKBKG* routes in the PI3K/AKT signaling. We also detected a down regulation *TP53* mRNA levels and a cell cycle perturbation (*via HDAC1*, *CDKN2C*, *GADD45A*, *CDC14A*, *CDC26* and *ANAPC5*). In parallel, a down regulation of genes of the pathways such as the TCA cycle, amino acid metabolism (down regulation of *ALDH7A1*, *DAO*, *LAP3*, *MAOA*, *MAOB*, *NAGS* for example in the arginine proline pathway), and sugar metabolism (down regulation of *ALDOB*, *MPI*, *TSTA3*, *SORD* in fructose and mannose metabolism and down regulation of *GALK2*, *HEXB*, *MPI*, *NAGK*, *TSTA3*, *UGP2* in amino sugar and nucleotide sugar metabolism) were observed (Figs 6A, 6B, 6C). This modulation was associated with the disturbances in the “genetic information processing” related pathways such as those involving ribosome and mRNA translation, and protein folding, sorting and degradation (Figs 6D and 6E). More specifically, we found a RNA transport mRNA levels down regulation (*via EIF1AX*, *EIF3B*, *EIF4G3*, *POP1*, *POP7*, *PRMT5*) and a down regulation in protein ubiquitin proteolysis (*via ANAPC5*, *CDC26*, *CUL4A*, *HERC3* *PPIL2*, *RHOBTB1*). Finally, we found an up regulation of the HIF-1 signaling *via FIGF*, *IGF1*, *PFKFB1*, *SERPINE1*, *TCEB2* mRNA levels.

In the 100vsctrl comparison, a modulation of the tight junctions’ pathway was specifically extracted in contrast to 10vsctrl *via* the down regulation at 100 μ M of *CGN*, *CLDN2*, *GNAI1*, *IGSF5*, *MAGI3*, *PPP2R1B*, *SPTAN1* mRNA when compared to controls (fold change and p-values are presented in supplement table 2). A down regulation in

the tryptophan, leucine, isoleucine, valine metabolism pathways was detected. Weak perturbations (on contrary to 10 μ M exposure) of the pathways related the TCA cycle, sugar metabolism, and protein processes was observed.

Based on these IPA and Kegg treatments, we propose two synthetic representations of the mechanism of action of flutamide, at 10 μ M and 100 μ M exposures, as shown in Figs 7A and 7B.

4. Discussions

Absorption Distribution Metabolism and Elimination genes are enhanced in microenvironment and microfluidic cultures (Sivaraman et al., 2005; Prot et al., 2011; Legendre et al., 2013). The maintenance of the drug metabolism genes were used to predict hepatic clearances (Novik et al., 2010; Chao et al., 2009; Baudoin et al., 2014). Integrations of transcriptomics, proteomics and metabolomics profiles from cell lines (such as HepG2/C3a and MDCK) in microfluidic cultures have demonstrated the potential to investigate the mechanism of xenobiotic toxicity (Choucha et al., 2012; Prot et al., 20). In this paper, we have successfully extended our feasibility study of our microfluidic methodology for biological investigations by integrating the transcriptomics profiles of rat primary hepatocytes when exposed to flutamide. Our results illustrated the possibility to culture primary cells and to collect pertinent data for mechanistic analysis. Using rat hepatocytes, we found three types of cellular response to the two flutamide treatments. The responses corresponded to a common flutamide response and two specific ones for each exposure conditions.

Commonly to both treatments, we found a down regulation of the Ppar signaling and of the fatty acid and lipid metabolism signaling. This type of down regulation has been already observed as a cell stress response in defense to the increase of Reactive Oxygen Species (Cabrero et al., 2002). Furthermore this down regulation was concomitant in the biochips with activation of *NFKB* related genes (such as *IKBKB* and *NFKB2* at 10 μ M, and *NFKB2* at 100 μ M) as reported in literature (Cabrero et al., 2002). In both exposure cases, we detected mitochondrial disturbance illustrated by the

perturbation of *mGSTA3*, *NDUFA9*, *NDUFA10*, *APAF1* and *mGSTA3*, *NDUFB4*, *LHPP*, *HTRA2*, *SLC25A4*, *APAF1* at 10 μ M and 100 μ M respectively. These results may appear consistent with the literature in which flutamide was presented as blocking electron transfer in the mitochondria (Coe *et al.*, 2006; Kashimshetty *et al.*, 2009). The mitochondrial disturbance has been related to a subsequent disturbance in cells such as in calcium homeostasis (Rasola *et al.*, 2011), illustrated in our study *via PSEN2* gene down regulation. Mitochondrial disturbances are also related to the modulation of some heat shock genes (Fulda *et al.*, 2010), to the LXR/RXR modulation (Alaynick, 2008), to the Ppar signaling (Anderson *et al.*, 2004) and in the lipid metabolism and fatty acid oxidation (Degli Esposti *et al.*, 2012) that appeared consistent with our results. However alamar blue levels in our tests at 10 and 100 μ M were increased when compared to controls. This result can illustrate an alternative respiration process (*via* complex II and III in the mitochondria, Metha *et al.*, 2008, or *via* glycolysis bypass, Coe *et al.*, 2007) associated with alamar blue reduction by cytosol or microsomal enzymes (Morten *et al.*, 2013, Gonzalez *et al.*, 2001; Petrenko *et al.*, 2005). Another route of exploration for a common response was to search for the potential effect of hydroxyflutamide itself. Despite hydroxyflutamide being a well-known anti-androgen, we did not identify specific disturbances related to the androgen pathway in our study. Finally, when compared to others *in vitro* flutamide hepatic characterization (Coe *et al.*, 2007), we consistently found modulated expression of genes associated with oxidative phosphorylation, fatty acid β -oxidation, antioxidant defense, and cell death pathways.

At 10 μ M of flutamide, we observed a global cellular defense response and a down regulation of mRNA levels related to basal cell functions. The mechanisms related to cell survival (*via* the AKT/PI3K and MAPK signaling up to the p53 signaling, Fig. 5A) were activated. Under stress conditions, this network played a part in stopping the cell cycle and enhancing the cellular repair mechanism. Nevertheless at the 24h time point, the overall response appeared to illustrate a down regulation of the pro-apoptotic signaling and pro survival activation. In addition, a down regulation of two heat shock proteins mRNA levels has been found (HSP40 and HSP70). It has been reported that general protein transcription and translation are halted in the initiation of the heat shock response. The chaperone proteins, such as HSP40 and HSP70, are involved through

inhibition of cell death pathways (by preventing protein aggregation for instance, or by forming co-chaperone complex modulating apoptosis, Fulda *et al.*, 2010). This might be consistent with the modulation of the protein network (Figs 6D and 6E) that we highlighted at 10 μ M. However, additional proteomic analysis and other time endpoint would be required to gain additional insight on this process as far as the perturbation found in the microarray was not correlated at the functional level (albumin and urea synthesis were not decreased in our flutamide exposures). After 24h of 10 μ M treatment, the activation of several cell defense routes (ROS responses, PI3K/AKT responses, heat shock response) may explain the limitation of the toxicity insofar as limited cell death was observed when compared to controls and to treatment with 100 μ M. This is coherent with the levels of the metabolic ratio illustrating a high flutamide biotransformation and the glutathione conjugations leading to detoxication of the drug and its metabolites. This is also confirmed by the calcein AM - PI double staining and the ROS staining by DCFDA at 10 μ M. Finally, the overall 10 μ M response was associated with an up regulation of the HIF-1 signaling (*via FIGF, IGF1, PFKFB1, SERPINE1, TCEB2* mRNA levels) illustrating high oxygen request.

At present, it is difficult to state whether the disturbance in sugar, amino acid and protein metabolism pathways at 10 μ M is a response due to cell defense activation (namely a reduction of none necessary biological processes and a subsequent reduction of the protein transcription and translation) or due to a specific response to flutamide. It has effectively been reported that flutamide modulates extracellular sugar uptake and the sugar metabolism routes (Naftalin *et al.*, 2003; Coe *et al.*, 2007). In our experiments, at the transcriptomic levels, we did not detect *GLUT1* glucose receptor modulation, and the glycolysis pathway was not itself disturbed for both concentrations. However, the low glucose consumption and the down regulation of sugar and amino acid metabolism pathways results at 10 μ M of flutamide appeared consistent with our previous metabolomics profiling in human liver HepG2/C3a in which extracellular glucose and amino acid uptakes were reduced at similar exposure conditions (Choucha *et al.*, 2013b). In parallel, we found intense glucose consumption at 100 μ M without any disturbance in sugar homeostasis when compared to controls. As we observed a transcriptomic modulation in the sugar pathways only at 10 μ M, it seems that our

observations are a dose dependent response but not an illustration of specific glucose transporter binding by flutamide.

At 100 μ M we observed a switch in the stress response from “apoptotic survival response” to “necrotic response”. At the biochip level it was first detected by a reduction in the number of cells collected. In addition, the lower metabolic ratios illustrated a saturation of the flutamide metabolism (flutamide metabolism saturation, *via* a *K_m* value reported between 2.48 and 4.1 μ M and a *V_{max}* value ranging between 200 and 472 pmol/min/mg, have been reported by Sjorgren et al., 2009). This led to a weak detoxication process and thus to maintaining a high level of flutamide in the culture medium (metabolism analysis) or inside the cell cytosol. At the transcriptomic level, the necrosis was associated with the desperation of the “protein degradation network” route and of most of the bridges in the “survival/apoptosis” pathways (Fig 5B, Fig 7B) whereas ROS cell stress response was maintained. Survival cell responses can be switched to necrosis during intense oxidative stress by two types of mechanisms: cellular ATP level depletion or caspase inactivation due to ROS accumulation at active sites (Fulda *et al.*, 2010). Maintaining the high level of flutamide, due to a lack of its biotransformation, may thus play a part in modulating mitochondrial ATP production. After 24h of 100 μ M treatment, the systemic stress led to significant cell death, illustrated by the reduction in the final cell number, the PI positive cells and the level of ROS. Specifically, at the transcriptomic level, the cellular organization appeared to be specifically altered as shown by the down regulation of the tight junction pathway. This result correlated with the hepatic aggregation morphologies and cell culture deterioration that we observed.

Then, we compared our *in vitro* data with the *in vivo* report performed on rats and mice. In our *in vitro* model, we found a reduction in hydroxyflutamide production at 100 μ M when compared to the 10 μ M treated cases. This was consistent with the observations made by Wang *et al.* 2005 and Matsuzaki *et al.*, 2006 in which giving rats flutamide induced liver CYP1A2 expression (protein, mRNA, activity) in a dose-dependent manner (this was also reported *in vitro* by Shet *et al.* 1997). *In vivo*, the gene response of the flutamide appeared to be a classical Ahr ligand response (*via* the substantial modulation of 15 genes over the consensus of 40 genes involved in the Ahr

pathway, Coe *et al.*, 2006). The flutamide also contributed to a down-regulation of the c-fos gene and modulated about 50 ADME-related genes including CYP2B and CYP3A (Coe *et al.*, 2006). Although, we observed down regulation by flutamide of *Ahr* related genes (inconsistently with *in vivo* rat tests of Coe *et al.*, 2006), we measured an increasing *CYP1A* activity, as demonstrated by the EROD assays. We also found with the microfluidic model the ADME genes modulation and an increase in CYP3A and CYP2C as observed *in vivo* (as shown table 2 at 10 μ M). Despite in the biochips we did not detect any similar direct c-fos down-regulation, we found a significant modulation in the related pathways, such as the MAPK signaling. However, the disruption of liver tissue integrity and ischaemia-reperfusion injury, both occurring during the isolation procedure, are reported to activate inflammatory and proliferative responses, mediated by nuclear factor kappaB and mitogen-activated protein kinase, respectively (Fraczek *et al.*, 2013). In addition, pentobarbital used for the extraction is known to cause induction of specific cytochromes including *CYP1A2* (Sakuma *et al.*, 1999). Consequently, the biochip cultures did not yet eliminate all common afferent drawbacks of *in vitro* cultures. Therefore, potential cross talks between several phenomena still conduct to the necessity of wider investigation with the biochips for more pertinent *in vivo* extrapolations.

5. Conclusion

In summary, we investigated the metabolism, biochemical functions and transcriptomic profiles of the effect of two flutamide concentrations on rat hepatocytes cultivated in microfluidic biochips. The hepatic response to 10 μ M flutamide exposure led to a pro-survival stress response. The response to 100 μ M flutamide exposure resulted in necrotic activation. This result demonstrated the potential for extracting from the liver biochip cultures certain typical toxicity profiles. As additional results, we proposed two integrated networks of toxicity in rat hepatocytes after 24h of exposure to 10 μ M and 100 μ M of flutamide. Nevertheless, additional functional measurements of specific biomarkers (such as quantification of ROS levels, caspases, and quantitative glutathione depletion) are required to confirm our metabolic and transcriptomic profilings. Flutamide

has idiosyncratic specific toxicity in humans that we could not detect in the present culture model because of the used of rat cells. However, the liver microfluidic biochip cultures might be adequate new tools for reproducing various types of liver and hepatocyte physiology (such as liver zonation, enhanced drug metabolism activities, etc...) using human cells. Better *in vitro* models may help to resolve and to address the idiosyncratic particularity especially by repeating our experiments with several human primary hepatocytes donors.

Acknowledgments:

This work was supported by the “Fondation pour la Recherche et l’Innovation” at the Université de Technologie de Compiègne (project ToxOnChip), and by the UTEAM-Carnot grant (project Parachip).

References

- Aizawa, Y., Ikemoto, I., Kishimoto, K., Wada, T., Yamazaki, H., Ohishi, Y., Kiyota, H., Furuta, N., Suzuki, H. , Ueda, M. (2003). Flutamide-induced hepatic dysfunction in relation to steady-state plasma concentrations of flutamide and its metabolites, *Molecular and Cellular Biochemistry*. 252:149–156.
- Alaynick W., (2008) Nuclear receptors, mitochondria and lipid metabolism, *Mitochondrion*,8:329-337
- Alegret M, Sánchez R, Adzet T, Laguna J and Vazquez Carrera M, Increased Reactive Oxygen Species Production Down-regulates Peroxisome Proliferator-activated α Pathway in C2C12 Skeletal Muscle Cells (2002) *The journal of biological chemistry*. 277: 10100–10107

552 Anderson S, Dunn C, Laughter A, Yoon L, Swanson C, Stulnig T, Steffensen K,
 553 Chandraratna R, Gustafsson J, Corton C (2004) Overlapping Transcriptional Programs
 554 Regulated by the Nuclear Receptors Peroxisome Proliferator-Activated Receptor,
 555 Retinoid X Receptor, and Liver X Receptor in Mouse Liver, *Mol Pharmacol* 66:1440–
 556 1452

557 Anjum, S., Swan, S.K., Lambrecht, L.J., Radwanski, E., Cutler, D.L., Affrime, M.B., and
 558 Halstenson, C.E. (1999). Pharmacokinetics of flutamide in patients with renal
 559 insufficiency. *British Journal of Clinical Pharmacology*. 47: 43-47.

560 Bains W. (2004) Failure rates in drug discovery and development: will we ever get any
 561 better? *Drug Discovery World Fall 2004, Business*, 1-18

562 Baudoin R, Griscom L, Prot JM, Legallais C, Leclerc E. (2011). Behavior of HepG2/C3A
 563 cell cultures in a microfluidic bioreactor, *Biochemical Engineering Journal*, 53:172–181

564 Baudoin R, Alberto G, Legallais C, Leclerc E (2012) Parallelized microfluidic biochips in
 565 multi well plate applied to liver tissue engineering. *Sensors and Actuators B*, 173: 919–
 566 926

567 Baudoin R, Prot JM, Nicolas G, Brocheton J, Brochot C, Legallais C, Benech H, Leclerc E
 568 (2013) Evaluation of seven drug metabolism and clearances by cryopreserved Human
 569 primary hepatocytes cultivated in microfluidic biochips, *Xenobiotica*, 43: 140-152

570 Baudoin R, Legendre A, Jacques S, Cotton J, Bois F, Leclerc E (2014) Evaluation of a
 571 Liver Microfluidic Biochip to Predict *In Vivo* Clearances of Seven Drugs in Rats, *Journal*
 572 *of Pharmaceutical Sciences* 103:706–718

573 Chao P, Maguire T, Novik E, Cheng KC, Yarmush ML. (2009). Evaluation of a
 574 microfluidic based cell culture platform with primary human hepatocytes for the
 575 prediction of hepatic clearance in human, *Biochemical pharmacology* 78: 625-632

576 Cheng S, Prot JM, Leclerc E, Bois FY. (2012). Zonation-related pathways in human
 577 hepatocellular carcinoma cells in dynamic vs. static culture microenvironments, *BMC*
 578 *genomic*, 13: 54-64

579 Choucha-Snouber L, Aninat C, Griscom L, Madalinski G, Brochot C, Poleni PE, Razan F,
 580 Guguen Guillozo C, Legallais C, Corlu A, Leclerc E (2013a) Investigation of ifosfamide
 581 nephrotoxicity induced in a liver kidney co-culture biochip, *Biotechnology and*
 582 *Bioengineering*, 110, 597-608, 2013

583 Choucha Snouber L, Bunescu A, Legallais C, Brochot C, Dumas ME, Elena-Herrmann B
 584 and Leclerc E (2013b) Metabolomics-on-a-chip of hepatotoxicity induced by anticancer
 585 drug flutamide and its active metabolite hydroxyflutamide using HepG2/C3a microfluidic
 586 biochips, *Toxicological Science* , 132:8-20

587 Coe, K., Jiav, Y., Ho, H., Rademacher, P., Bammler, T., Beyer, R., Farin, F., Woodke,
 588 L., Stephen, R., Plymate, S., Fausto, N., Nelson, S. (2007). Comparison of the
 589 Cytotoxicity of the Nitroaromatic Drug Flutamide to Its Cyano Analogue in the
 590 Hepatocyte Cell Line TAMH: Evidence for Complex I Inhibition and Mitochondrial
 591 Dysfunction Using Toxicogenomic Screening. *Chem Res Toxicol.* 20: 1277–1290.

592 Coe, K., Nelson S., Ulrich R., He Y., Dai X., Cheng O., Caguyong M. Roberts C., Slatter
 593 G, (2006). Profiling the hepatic effects of flutamide in rats: a microarray comparison with
 594 classical aryl hydrocarbon receptor ligands and atypical CYP1A inducers, *Drug Metab*
 595 *Dispo.* 34: 1266–1275.

596 Degli Esposti D., Hamelin J, Bosselut N, Saffroy R, Sebah M, Pommier A, Martel C,
 597 and Lemoine A (2012) Mitochondrial Roles and Cytoprotection in Chronic Liver Injury
 598 *Biochemistry Research International*, ID 387626, 1-16

599 Fraczek J, Bolleyn J, Vanhaecke T, Rogiers V, Vinken M. (2013) Primary hepatocyte
 600 cultures for pharmaco-toxicological studies: at the busy crossroad of various anti-
 601 dedifferentiation strategies., *Arch Toxicol.* 87:577-610

602 Fulda S., Gorman A., Hori Osamu, Samali A. (2010) Cellular stress response: cell
 603 survival and cell death, *Int J. of cell biology*, 1-23

604 Gonzalez RJ, Tarloff JB. (2001) Evaluation of hepatic subcellular fractions for Alamar
 605 blue and MTT reductase activity. *Toxicol In Vitro.*15:257-9.

606 Iwanaga T, Nakakariya M, Yabuuchi H, Maeda T, Tamai I. (2007) Involvement of bile
 607 salt export pump in flutamide-induced cholestatic hepatitis. *Biol Pharm Bull*, 30: 739-44

608 Kashimshetty, R., Desai, V.G., Kale V.M., Lee, T., Moland, C.L., Branham, W.S., New,
 609 L.S., Chan, E.C., Younis, H., Boelsterli, U.A. (2009). Underlying mitochondrial
 610 dysfunction triggers flutamide-induced oxidative liver injury in a mouse model of
 611 idiosyncratic drug toxicity. *Toxicol Appl Pharmacol.* 238:150-159.

612 Kostrubsky SE, Strom SC, Ellis E, Nelson SD, Mutlib AE (2007) Transport, metabolism,
613 and hepatotoxicity of flutamide, drug-drug interaction with acetaminophen involving
614 phase I and phase II metabolites. *Chem Res Toxicol*, 20: 1503e12.

615 Lee YF, Lin WJ, Huang J, Messing EM, Chan FL, Wilding G, Chang C.(2002) Activation
616 of mitogen-activated protein kinase pathway by the antiandrogen hydroxyflutamide in
617 androgen receptor-negative prostate cancer cells, *Cancer Res.* 62:6039-44.

618 Legendre A, Baudoin R, Alberto G, Paullier P, Naudot M, Bricks T, Brocheton J,
619 Jacques S, Cotton J and Leclerc E (2013) Metabolic characterization of primary rat
620 hepatocytes cultivated in parallel microfluidic biochips, *Journal of Pharmaceutical*
621 *Science*, *J Pharm Sci* 102: 3264-76.

622 Matsuzaki Y, Nagai D, Ichimura E, Goda R, Tomura A, Doi M, Nishikawa K (2006)
623 Metabolism and hepatic toxicity of flutamide in cytochrome P450 1A2 knockout SV129
624 mice, *J Gastroenterol.* 41:231–239

625 Mehta R, Chan K, Lee O, Tafazoli S, O'Brien P., 2008, Drug associated Mitochondrial
626 toxicity in Drug-Induced Mitochondrial Dysfunction, Editors James A. Dykens, Yvonne
627 Will

628 Morten K, Badder L and Knowles H (2013) Differential regulation of HIF-mediated
629 pathways increases mitochondrial metabolism and ATP production in hypoxic
630 osteoclasts, *J Pathol.* 229: 755–764

631 Naftalin, R, Afzal, I., Cunningham, P., Halai, M, Ross, C., Salleh, N., Milligan, S. (2003).
632 Interactions of androgens, green tea catechins and the antiandrogen flutamide with the
633 external glucose-binding site of the, human erythrocyte glucose transporter GLUT1.
634 *British Journal of Pharmacology.* 140: 487–499.

635 Novik E, Maguire TJ, Chao P, Cheng KC, Yarmush ML. (2010). A microfluidic hepatic
636 coculture platform for cell-based drug metabolism studies. *Biochemical Pharmacology*
637 79:1036-1044

638 Petrenko YA, Gorokhova NA, Tkachova EN, Petrenko AY. (2005) The reduction of
639 Alamar Blue by peripheral blood lymphocytes and isolated mitochondria. *Ukr Biokhim*
640 *Zh.* 77:100-5.

641 Powers MJ, Janigan D, Wack KE, Baker, Stolz DB, Griffith L. (2002). Functional
642 behavior of primary Rat liver cells in a three-dimensional perfused microarray bioreactor.
643 Tissue Engineering 8:499-508

644 Prot JM, Briffaut AS, Letourneur F, Chafey P, Merlier F, Grandvalet Y, Legallais C,
645 Leclerc E. (2011a). Integrated proteomic and transcriptomic investigation highlights
646 original insight into paracetamol toxicity in liver biochip, PlosOne, 6, 21268

647 Prot JM, Aninat C, Griscom L, Razan F, Brochot C, Guguen Guillouzo C, Legallais C,
648 Corlu A, Leclerc E. (2011b) Improvement of HepG2/C3a cell functions in a microfluidic
649 biochip, Biotechnology and Bioengineering, 108:1704-1715

650 Prot J.M., Bunescu A., Elena-Hermann B., Aninat C., Choucha Snouber L, Griscom L.,
651 Bois, F., Legallais, C., Brochot, C., Corlu, A. , Dumas, M.D., Leclerc, E. (2012)
652 Predictive toxicology using systemic biology and liver microfluidic “on chip” approaches:
653 Application to acetaminophen injury. Toxicology and Applied Pharma, 259: 270-280

654 Radwanski E, Perentesis G, Symchowicz S, Zampaglione N. (1989) Single and multiple
655 dose pharmacokinetic evaluation of flutamide in normal geriatric volunteers. J Clin
656 Pharmacol. 29:554-558.

657 Rasola A and Bernardi P (2011) Mitochondrial permeability transition in Ca²⁺-
658 dependent apoptosis and necrosis, Cell Calcium, 50:222–233

659 Sakuma T., Ohtake M, Katsurayama Y, Jarukamjorn K, Nemuto N (1999) Induction of
660 CYP1A2 by Phenobarbital in the Livers of Aryl Hydrocarbon-Responsive and -
661 Nonresponsive Mice *Drug Metab Dispo.* 27:379-384

662 Schrauwen P and Hesselink M (2004) Oxidative Capacity, Lipotoxicity, and
663 Mitochondrial Damage in Type 2 Diabetes, Diabetes. 53:1412-1417

664 Schulz, M., Schmoldt, A., Donn, F., Becker, H. (1988). The Pharmacokinetics of
665 Flutamide and Its Major Metabolites after a Single Oral Dose and During Chronic
666 Treatment. European Journal of Clinical Pharmacology. 34: 633-636.

667 Seglen PO 1973. Preparation of rat liver cells. 3. Enzymatic requirements for tissue
668 dispersion. Exp Cell Res 82:391-398.

669 Shet, M., Mc Paul, M., Fisher, C., Stallings, N., Estabrook, R. (1997). Metabolism of the
670 antiandrogenic drug (flutamide) by human CYP1A2. Drug Metabolism and Disposition.
671 25 :1298-1303

672 Sivaraman, A., Leach, J.K., Townsend, S., Iida, T., Hogan, B.J., Stolz, D.B., Fry, R.,
 673 Samson, L.D., Tannenbaum, S.R., Griffith, L.G. (2005). A Microscale In Vitro
 674 Physiological Model of the Liver: Predictive Screens for Drug Metabolism and Enzyme
 675 Induction. *Current Drug Metabolism*. 6:569-592.

676 Sjogren E, Lennernas H, Andersson T, Gråsjö J, and Bredberg U (2009) The Multiple
 677 Depletion Curves Method Provides Accurate Estimates of Intrinsic Clearance (CL_{int}),
 678 Maximum Velocity of the Metabolic Reaction (V_{max}), and Michaelis Constant (K_m):
 679 Accuracy and Robustness Evaluated through Experimental Data and Monte Carlo
 680 Simulations, *DMD* 37:47–58.

681 Tilles A, Baskaran H, Roy P, Yarmush M, Toner M. (2001). Effects of oxygenation and
 682 flow on the viability and function of rat hepatocytes cocultured in a microchannel flat-
 683 plate bioreactor. *Biotech Bioeng*. 73:379-389

684 Toh, Y.C., Lim, T.C., Tai, D., Xiao, G., van Noort, D., Yu, H. (2009). A microfluidic 3D
 685 hepatocyte chip for drug toxicity testing. *Lab on Chip*. 9: 2026-2031.

686 Viravaidya K and Shuler ML (2004) Incorporation of 3T3-L1 cells to mimic
 687 bioaccumulation in a microscale cell culture analog device for toxicity studies.
 688 *Biotechnol. Prog* 20:590-597

689 Zhang, S., Tong, W., Zheng, B., Susanto, T., Xia, L., Zhang, C., Ananthanarayanan, A.,
 690 Tuo, X., Sakban, R., Jia, R., Iliescu, C., Chai, KH., McMillian, M., Shen, S., Leo, H.,
 691 Yu, H. (2011). robust high-throughput sandwich cell-based drug screening platform.
 692 *Biomaterials*. 32:1229-1241.

693 Wang HX, Ma XC, Deng QL, Li D (2002) Cytotoxicity of flutamide and 2
 694 hydroxyflutamide and their effects on CYP1A2 mRNA in primary rat hepatocytes, *Acta*
 695 *Pharmacol Sin*, 23 :562-566

696 Wang HX, Liu X, Xu C, Ma X, Long J, Li D (2005) Induction of liver cytochrome P450
 697 1A2 expression by flutamide in rats, *Acta Pharmacol. Sin*, 26 : 1382–1386

698 Welsbie DS, Xu J, Chen Y, Borsu L, Scher HI, Rosen N, Sawyers CL. (2009) Histone
 699 deacetylases are required for androgen receptor function in hormone-sensitive and
 700 castrate-resistant prostate cancer. *Cancer Res*. 69:958-66

Table 1: Most relevant pathways extracted by the Ingenuity analysis based on the microarray data.

Comparison	Pathway name	Pathway type	P-value
Control vs 10µM of Flutamide after 24h of cultures (899 genes)	LPS/IL-1 mediated inhibition of RXR function	Top canonical pathway	8.17×10^{-5}
	Acute Phase Response Signaling	Top canonical pathway	1.17×10^{-4}
	LPS/IL-1 mediated inhibition of RXR function	Top Tox List	7.96×10^{-5}
	Xenobiotic metabolism signaling	Top Tox List	2.9×10^{-4}
	Positive Acute Phase Response Proteins	Top Tox List	1.58×10^{-3}
	Fatty acid metabolism	Top Tox List	1.95×10^{-3}
Control vs 100µM of Flutamide after 24h of cultures (471 genes)	Fatty acid b oxidation I	Top canonical pathway	2.4×10^{-7}
	LPS/IL-1 mediated inhibition of RXR function	Top canonical pathway	5.93×10^{-7}
	Acute Phase Response Signaling	Top canonical pathway	6.03×10^{-6}
	Complement system	Top canonical pathway	7.35×10^{-6}
	LXR/RXR activation	Top canonical pathway	1.91×10^{-5}
	Fatty acid metabolism	Top Tox List	2.1×10^{-11}
	LPS/IL-1 mediated inhibition of RXR function	Top Tox List	2.26×10^{-7}
	Cytochrome P450 panel related to Fatty acid	Top Tox List	1.44×10^{-6}
	LXR/RXR activation	Top Tox List	2.38×10^{-5}

Table 2: Genes extracted by Kegg analysis concerning PI3K/AKT, MAPK and JAK/STAT signaling (fold changes are ± 1.5 and *p-values* are below 0.05; details are given in Supplement Tables 5 and 6). Underline genes denote up regulation.

	10µM flutamide	100µM flutamide
Networks and pathways	Gene symbol	Gene symbol
PI3K/AKT signaling	<u>BCL2L11</u> , <u>BCL2L13</u> , <u>CREB5</u> , <u>FIGF</u> , <u>FN1</u> , <u>GNG3</u> , <u>IGF1</u> , <u>IKBK</u> G, JAK2, OSMR, PCK2, <u>PDGFC</u> , STK11, TP53, TP53RK	<u>CREB5</u> , <u>FIGF1</u> , <u>FIGF2</u> , <u>FN1</u> , GYS2, ITGA6, JAK2, OSMR, PPP2R1B, <u>VEGF</u>
JAK/STAT signaling	CTF1, <u>DDIT3</u> , IL22RA1, IL23A, JKA2, OSMR, SOCS2, SOCS5, STAT1, STAT6	CTF1, IL22RA1, IL23A, JKA2, OSMR, SOCS2
MAPK signaling	<u>DUSP8</u> , <u>DDIT3</u> , <u>FLNA</u> , <u>FLNB</u> , <u>GADD45A</u> , <u>IKBK</u> G, NFKB2, MAP3K4, PPP3CB, RASA1, TP53, TP53RK	NFKB2, MAP3K4, MAP3K6, MKNK1, FIGF1, <u>FIGF2</u>

Table 3: Genes extracted by Kegg analysis concerning drug metabolism consensus,*mapping using ingenuity pathway analysis (fold changes are ± 1.5 and *p-values* are below 0.05; details are given in Supplement Tables 7 and 8). Underline genes denote up regulation.

	10 μ M flutamide	100 μ M flutamide
Networks and pathways	Gene symbol	Gene symbol
Drug and xenobiotic metabolism	ITPA, NAT1, ADH4, AOX1, MAOA, MAOB, AKR7A3, CYP2C9, CYP3A2, HNF4a, <u>G6PD</u> , GSTA3, <u>GSTK1</u> , GSTA4, <u>GSTT2</u> , MGSTA3, UGT1A6, UGT1A7c, UGT2B17, UGT2B28	AOX1, FMO5, GSTA3, <u>GSTK1</u> , <u>GSTT2</u> , GSTA4, HNF4a, MGST3, PXR
Glutathione metabolism	<u>G6PD</u> , GPX2, GSS, GSTA3, <u>GSTK1</u> , GSTA4, <u>GSTT2</u> , IDH1, LAP3, MGST3	GPX2, GSTA3, <u>GSTK1</u> , <u>GSTT2</u> , GSTA4, MGST3
Ppar signaling	ACSL3, ACSL5, ANGPTL4, <u>APOA2</u> , AQP7, CD36, CPT1A, CPT1B, PCK2, SCP2, <u>UBC</u>	ANGPTL4, <u>APOA2</u> , CD36, CPT1A, CPT1B, CYP4A11, CYP27A1, GK, HMGCS2, SCP2, <u>UBC</u> , SLC27A2
Ahr signaling*	ALDH6A1, ALDH7A1, APAF1, GSTA3, <u>GSTK1</u> , GSTA4, <u>GSTT2</u> , GSST2B, MGSTA3, UGT1A6, UGT1A7c, UGT2B17, UGT2B28	ALDH1A1, APAF1, GSTA3, <u>GSTK1</u> , <u>GSTT2</u> , GSTA4, MGST3, NCOA7, SUL1B1
Lipid and fatty acid	AGPAT2, ADH4, ALDH7A1, DGKZ, LIPC, MGLL, PPAP2C, CPT1A, CPT1B, ACSL3, ACSL5, PNPLA7, PTDSS2	ACAA2, ACADVL, AGPAT2, DGAT2, DGKZ, GK, LIPN1, MGLL, CPT1A, CPT1B, CYP4A11, ECHS1, ECI1, ECI2, HADH, HADHA
Bile acid synthesis	ABCB1, ABCC3, ABCC4, AKR1D1, AQP8, BAAT, <u>CYP3A2</u> , CYP39A1, HSD17B4, SCP2, HMGCR, SLC4A4	ABCB4, AQP8, ATPB1, BAAT, HMGCR, SCL10A2, SCLO1B3
ABC transporters	ABCA8, ABCA1, ABCB6, ABCB7, ABCC3, ABCC4, ABCC5	ABCB4
Steroid hormone	AKR1D1, <u>CYP3A2</u> , HSD17B6, UGT1A6, UGT2B17, UGT2B28	

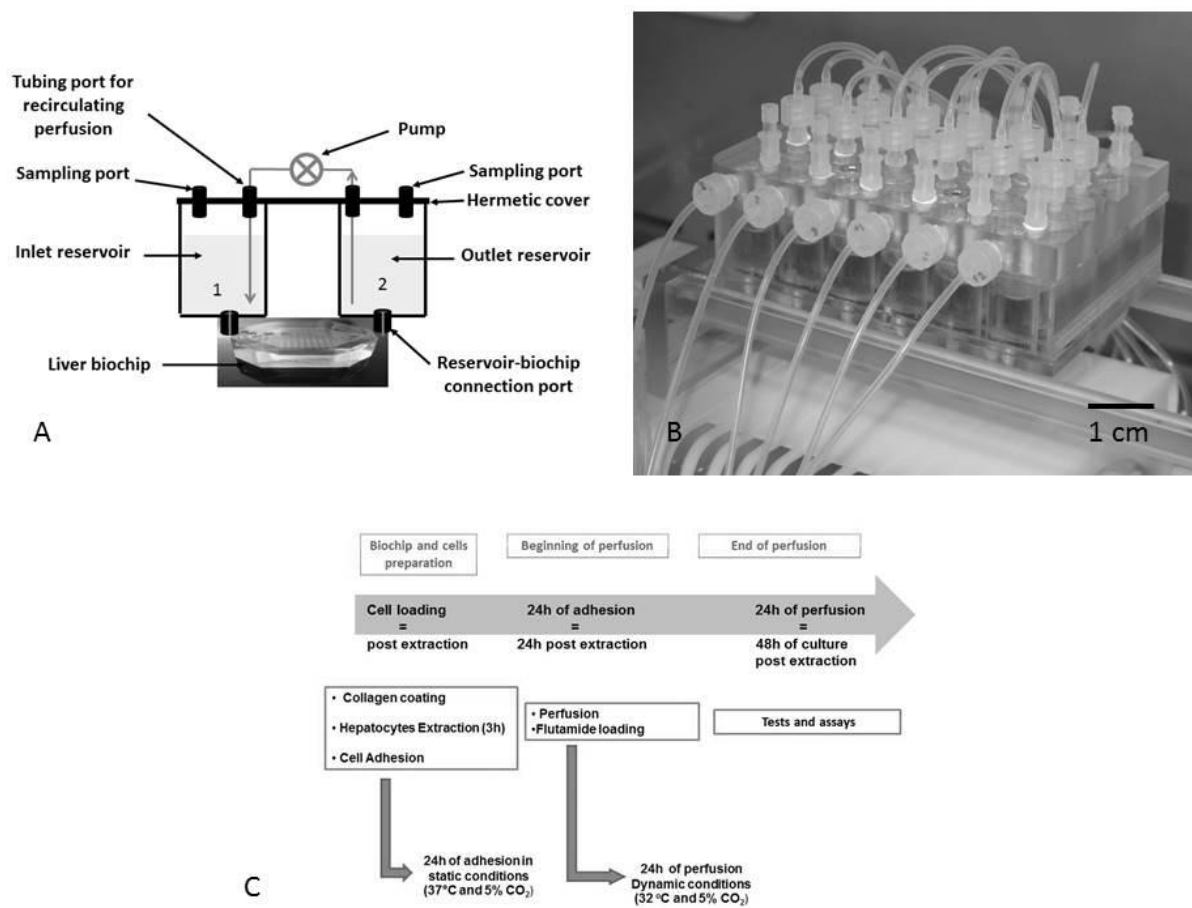


Figure 1: (A) Principle of the IDCCM biochip and perfusion cultures; (B) IDCCM box with working pump; (C) Experimental procedures.

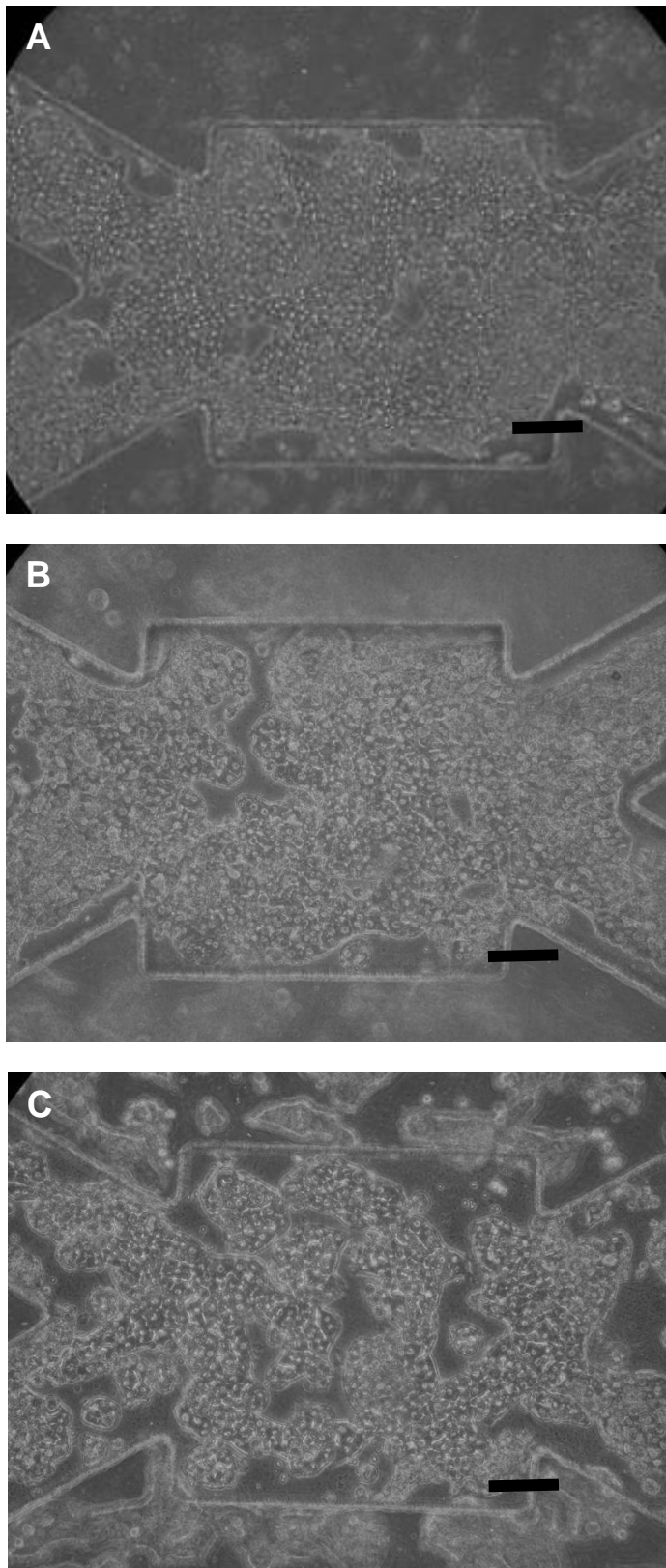


Figure 2: Hepatocyte morphologies in the IDCCM biochip at the end of the perfusion cultures; (A) controls; (B) after 24h of 10 μ M-flutamide; (C) after 24h of 100 μ M-flutamide. Scale bar is 100 μ m.

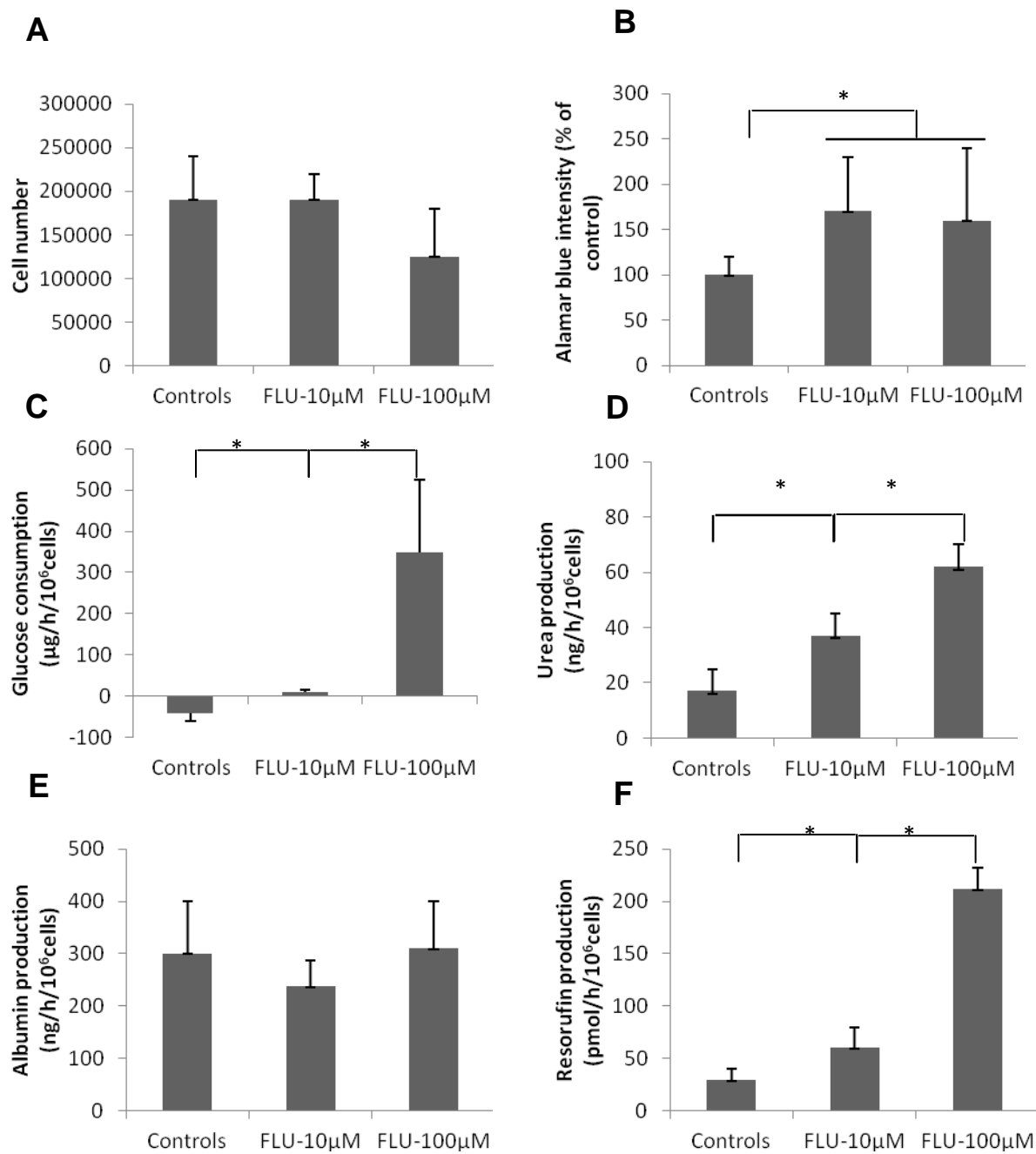


Figure 3: Comparison of control (vehicle 0.1% DMSO) of 10μM and of 100μM flutamide biochip cultures: (A) Final collected cell number; (B) Alamar blue metabolism; (C) Glucose consumption; (D) Urea production; (E) Albumin production; (F) Resorufin production *via* CYP1A activity (n=6 biochips, mean±SEM; * p < 0.05).

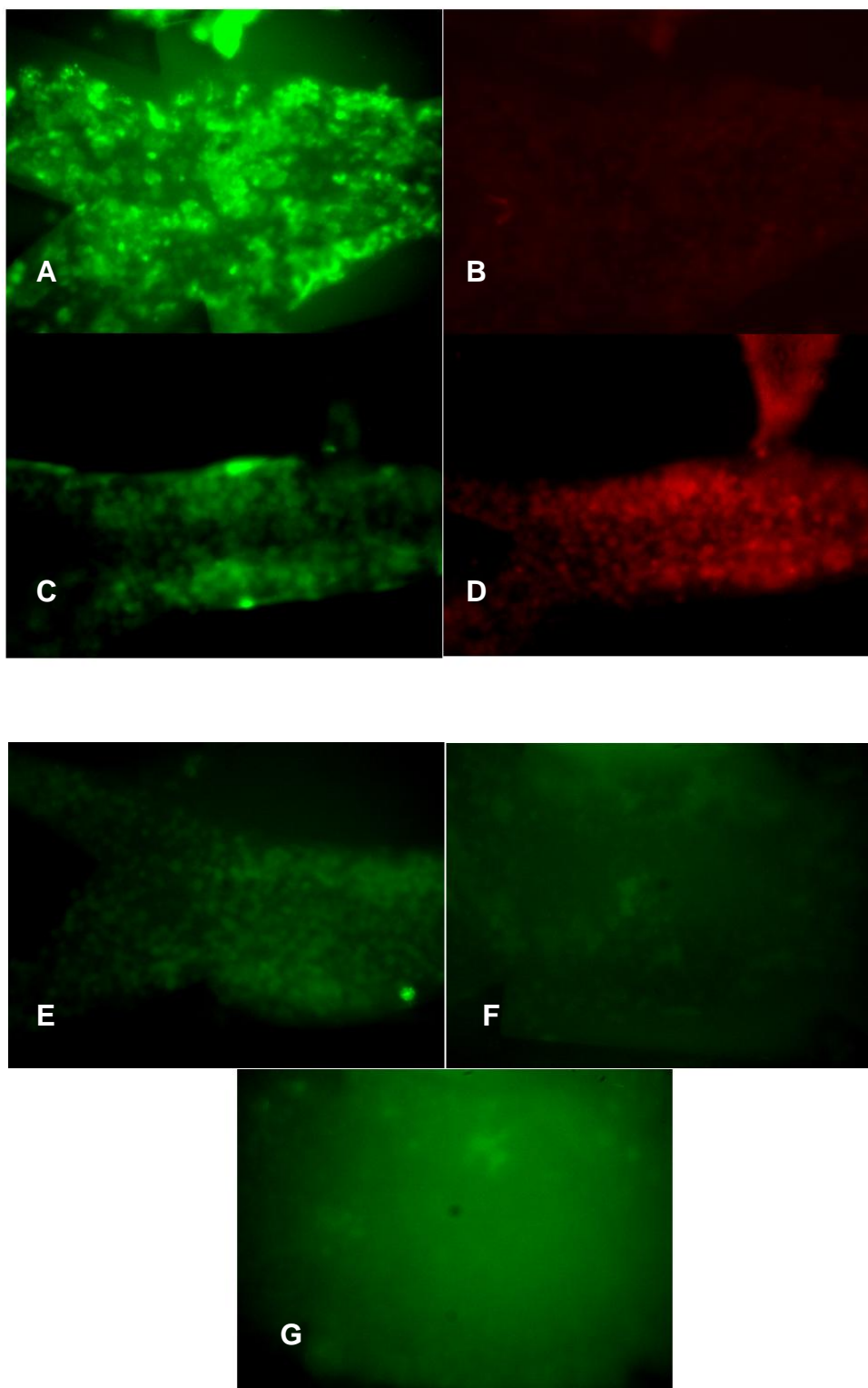


Figure 4: Calcein AM and propidium iodide double staining in biochips after 24h of flutamide exposures at 10µM (A, B) and of 100µM (C, D) ; ROS staining via DCFA probe in biochips after 24h of cultures in 100µM (E), in 10µM (F) and control (G)

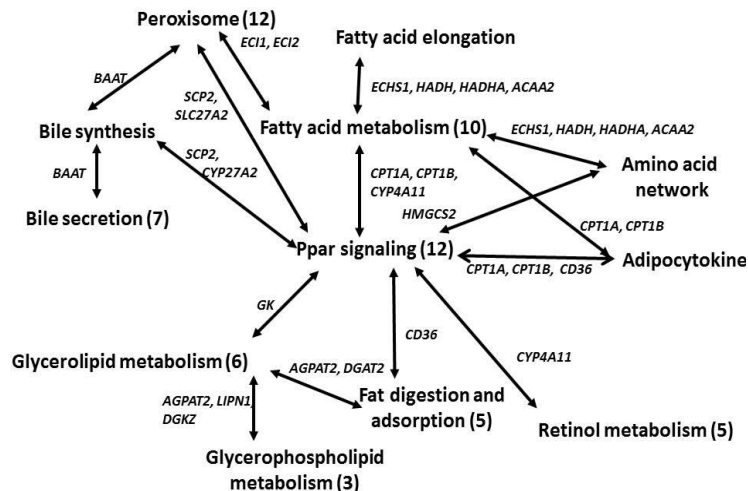
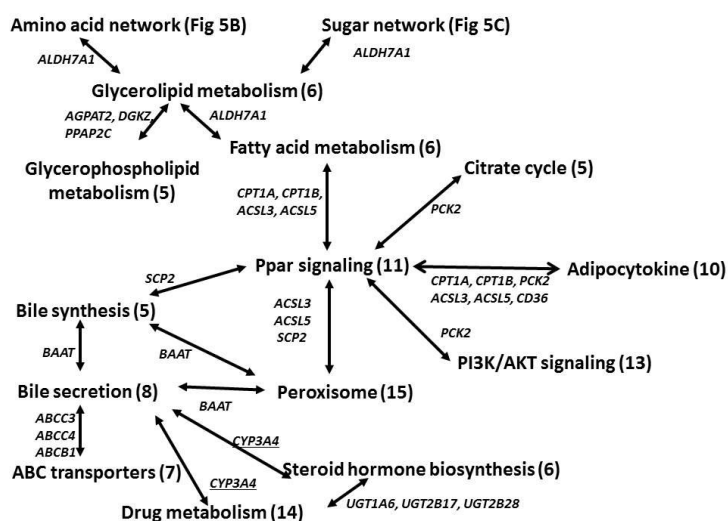
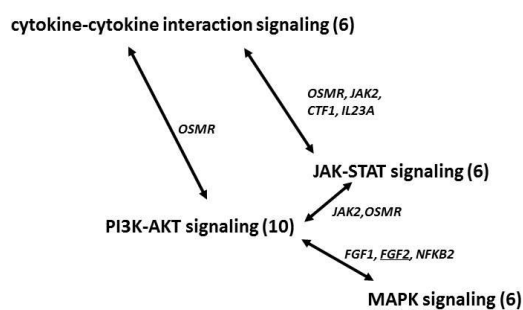
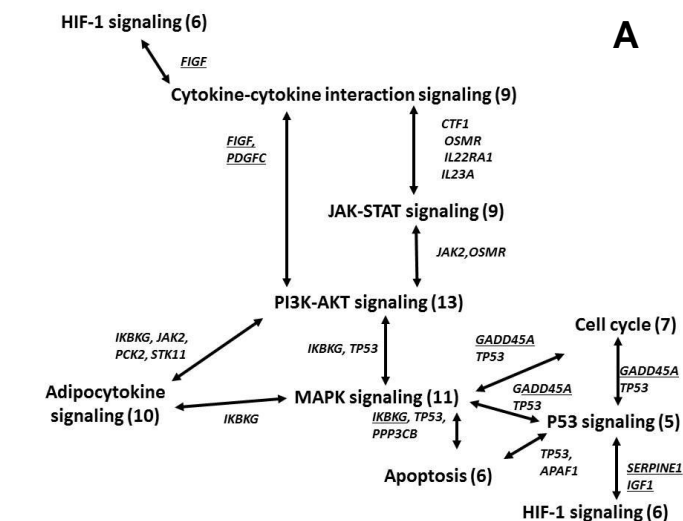


Figure 5: Network reconstructions; Survival/apoptosis networks at (A) 10 μ M and (B) 100 μ M; Lipid, fatty acid and Ppar signaling networks at (C) 10 μ M and (D) 100 μ M; common genes are used as bridges; fold changes are ± 1.5 and *p-values* are below 0.05; *GENE* = downregulated; *GENE* = upregulated; (number of gene in the pathways).

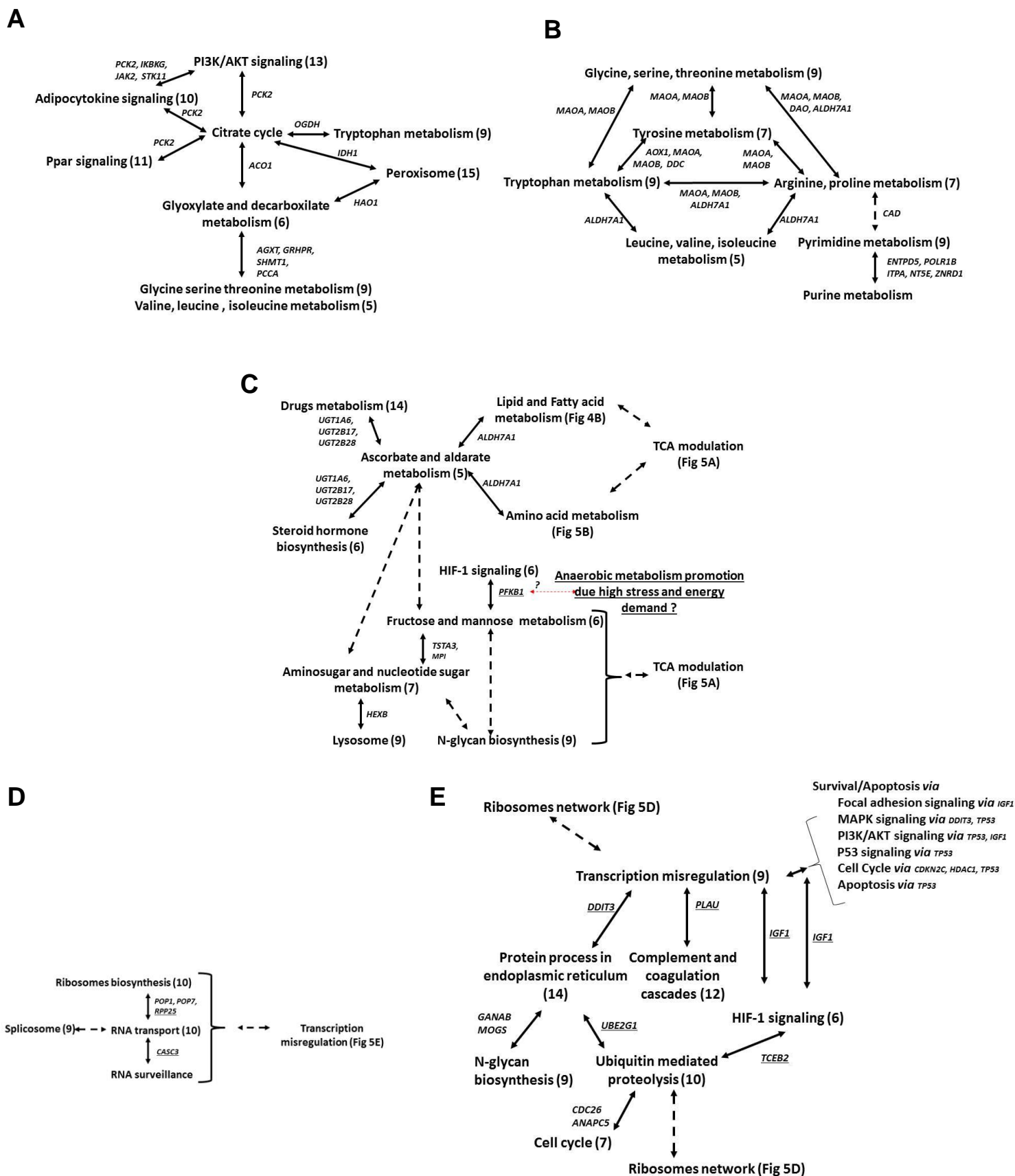
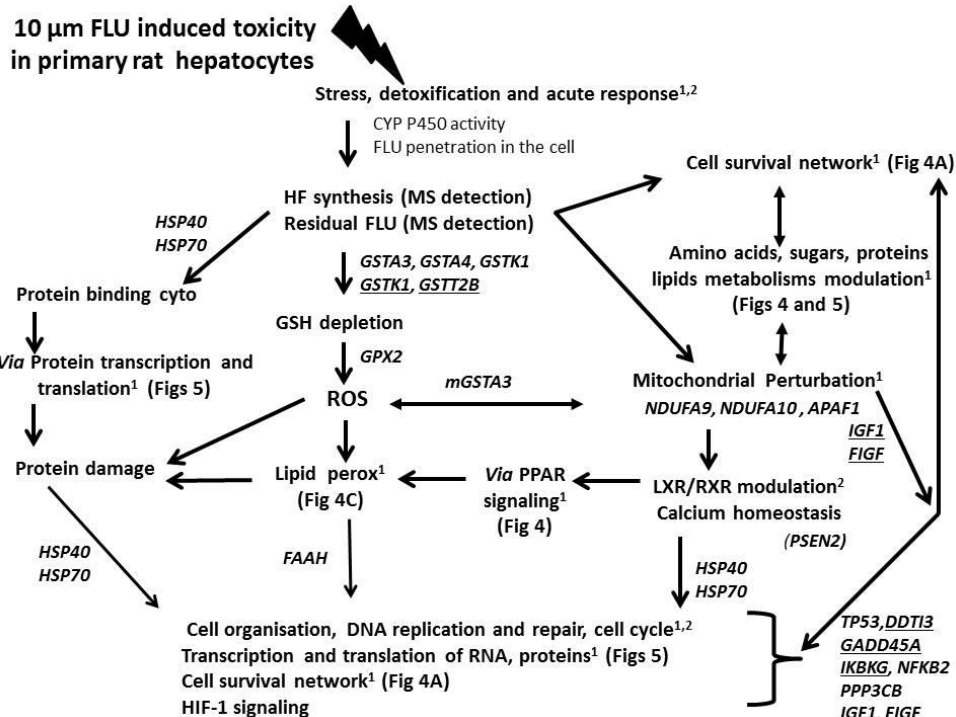


Figure 6: Network reconstructions at 10 μ M exposure; (A) TCA network, (B) amino acid metabolism network; (C) sugar network; (D) Ribosome network; (E) Protein network; common genes are used as

bridges; fold changes are ± 1.5 and *p-values* are below 0.05; *GENE* = downregulated; *GENE* = upregulated; (number of gene in the pathways).

A



B

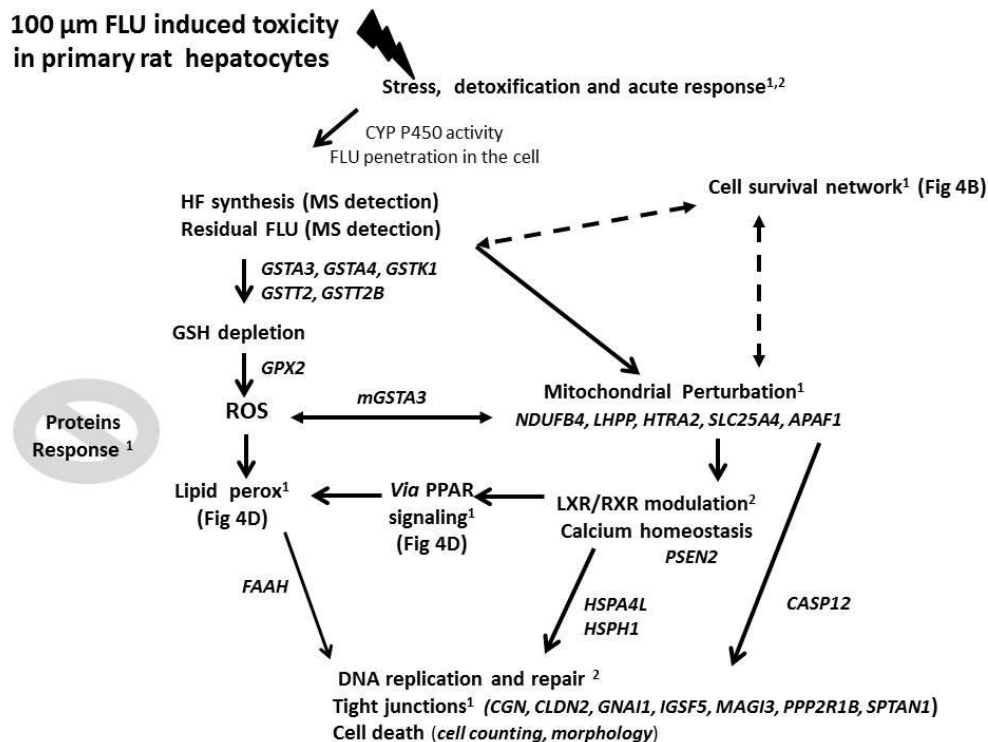
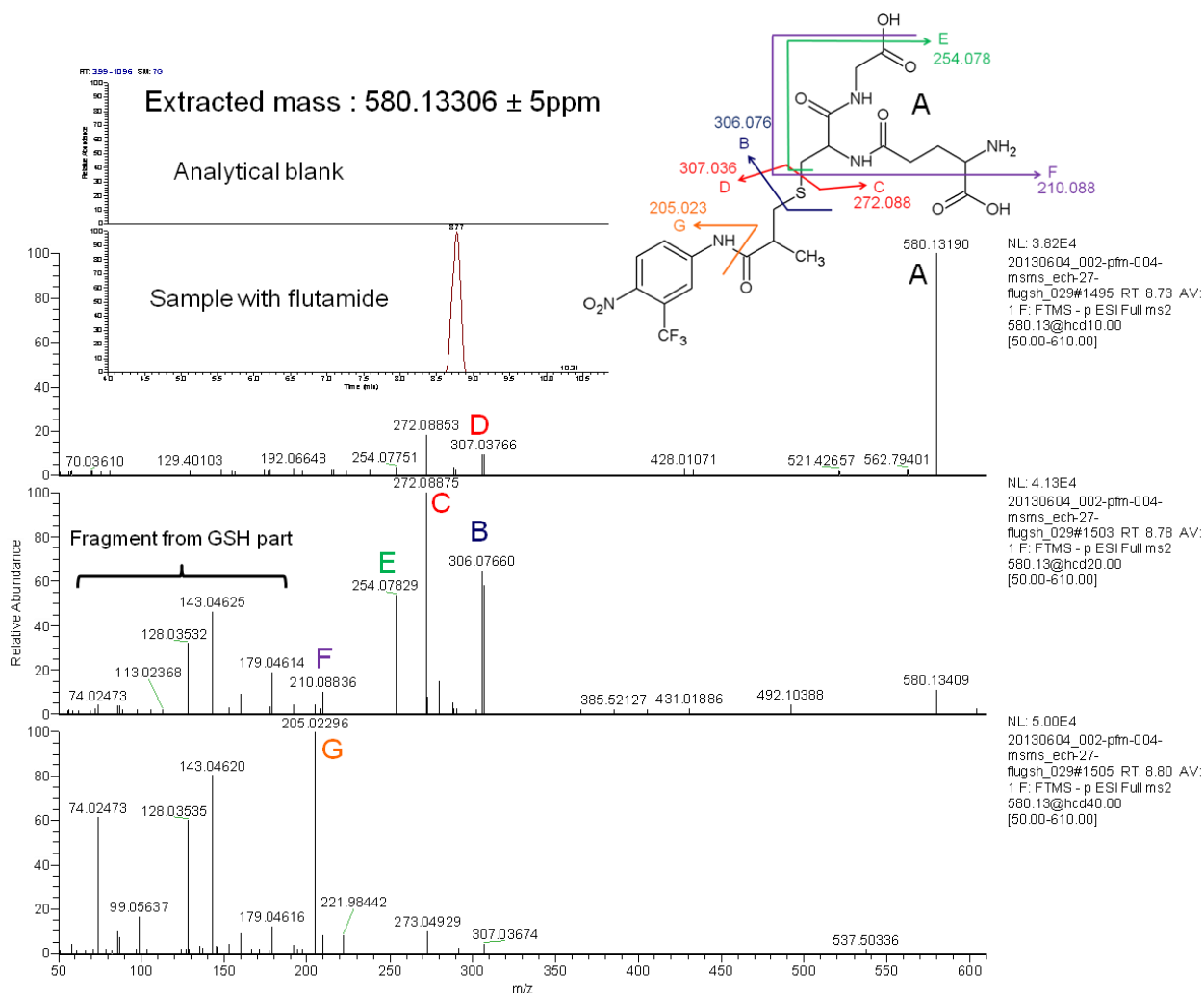


Figure 7: Global network reconstruction illustrating flutamide toxicity at 10 μ M (A) and 100 μ M (B). Superscript 1 denotes the network we elicited from the Kegg database; Superscript 2 denotes the network we elicited from the Ingenuity database. fold changes are ± 1.5 and p -values are below 0.05



Supplement Figure 1: Structural confirmation of the presence of flutamide covalently complexed with glutathione. The extract chromatogram shows the presence of the molecule in the sample, while the mass spectra from fragmentation experiments show two specific ion fragments D and G.